Nanoscale Horizons

ROYAL SOCIETY OF CHEMISTRY

COMMUNICATION

View Article Online
View Journal

Cite this: DOI: 10.1039/d5nh00441a

Received 26th June 2025,
Accepted 26th November 2025

DOI: 10.1039/d5nh00441a

rsc.li/nanoscale-horizons

Unlocking interstitial fluid for acute coronary syndrome diagnosis: ultrasensitive troponin I detection using imprinted polymer nanoparticles

Joshua Saczek, [ab] Amy Dann, [ab] Robert D. Crapnell, [c] Craig E. Banks, [c] Rhiannon E. Johnson, [d] Francesco Canfarotta, [d] Alan Thomson, [d] Azfar Zaman, [ef] Ioakim Spyridopoulos, [e] Katarina Novakovic, [a] Marloes Peeters [ab] and Jake McClements *[a]

This study presents the first detection of cardiac troponin I (cTnI), a vital biomarker for acute coronary syndrome diagnosis (ACS), in human interstitial fluid (ISF) collected *via* electroporation. Measurements were performed using molecularly imprinted polymer nanoparticles as synthetic recognition elements and a heat-transfer method within a microfluidic system, yielding results within 15–20 min. This approach demonstrated reliable cTnI quantification across a wide, physiologically relevant concentration range of 0.1 to 1000 pg mL^{-1} in spiked ISF, achieving an excellent detection limit of 1.85 ± 0.32 pg mL^{-1}. Comparisons with conventional patient sample fluids were conducted by repeating experiments with cTnI-spiked plasma and serum, which exhibited similar detection limits of 1.78 ± 0.28 and 1.80 ± 0.22 pg mL^{-1}, respectively. The developed sensor offers a rapid, highly sensitive, non-invasive, and cost-effective platform for point-of-care ACS diagnosis in ISF, potentially improving patient outcomes and easing healthcare burdens.

New concepts

Cardiac troponin I (cTnI) is a gold standard biomarker for diagnosing acute coronary syndrome (ACS). This study presents the first detection of cTnI in human interstitial fluid (ISF) using molecularly imprinted polymers (MIPs), representing a significant advancement in non-invasive ACS diagnosis. By integrating MIP nanoparticles (nanoMIPs) with a heat-transfer sensing method, the research demonstrates ultrasensitive and rapid detection of cTnI in ISF, a biofluid previously underutilized due to extraction challenges. Unlike conventional diagnostics that rely on invasive blood draws and centralized laboratories, this platform enables point-of-care testing with minimal sample volume and rapid measurements (15–20 minutes), while maintaining exceptional sensitivity. Moreover, the nanoMIP-thermal detection platform provides key advantages over existing MIP-based sensors, including excellent signal stability, no need for labels or redox probes, and minimal susceptibility to matrix effects. Comparative analyses in serum and plasma yielded results consistent with those obtained with ISF, validating the platform's high specificity across biological matrices. This work not only validates ISF as a viable medium for ACS diagnosis but also showcases the robustness of nanoMIP-based thermal sensing under clinically relevant conditions. The findings open new avenues for wearable, non-invasive monitoring technologies, offering transformative potential for early ACS diagnosis and applications in personalised healthcare.

1. Introduction

Acute coronary syndromes (ACS), comprising non-ST-elevation and ST-elevation myocardial infarction, commonly known as heart attacks, remain a leading cause of morbidity and mortality worldwide.[1,2] Early and accurate diagnosis of ACS is crucial for improving patient outcomes and reducing the overall burden of cardiovascular disease. For patients presenting with ST-elevation myocardial infarction (STEMI), the "golden hour" concept underscores the importance of rapid treatment, as delays in diagnosis and treatment significantly increase mortality rates; for every 30-minute delay in treatment, one-year mortality rises by 7.5%.[3] For non-ST-elevation myocardial infarction (NSTEMI), rapid diagnosis avoids delay in treatment and can enable early discharge in patients without a troponin rise. Despite technological advancements, current ACS diagnostic pathways in UK Accident and Emergency (A&E) departments are often slow, with a target turnaround time ranging from 1 to 24 h (Table S2), including a ~3 h period for

[a] Newcastle University, School of Engineering, Merz Court, Claremont Road, NE1 7RU Newcastle Upon Tyne, UK. E-mail: jake.mcclements@newcastle.ac.uk, katarina.novakovic@newcastle.ac.uk
[b] School of Engineering, University of Manchester, Nancy Rothwell Building, East Booth Street, M13 9QS Manchester, UK. E-mail: joshua.saczek@manchester.ac.uk, amy.dann@postgrad.manchester.ac.uk, marloes.peeters@manchester.ac.uk
[c] Faculty of Science and Engineering, Manchester Metropolitan University, Chester Street, M1 5GD Manchester, UK. E-mail: R.Crapnell@mmu.ac.uk, C.Banks@mmu.ac.uk
[d] Tozaro, The Exchange Building, Colworth Park, Sharnbrook, MK44 1LQ Bedford, UK. E-mail: rhiannon_e_johnson@outlook.com, francesco.canfarotta@tozaro.com, alan.thomson@tozaro.com
[e] Translational and Clinical Research Institute, Newcastle University, NE7 7DN Newcastle upon Tyne, UK. E-mail: azfar.zaman@nhs.net, ioakim.spyridopoulos@newcastle.ac.uk
[f] Freeman Hospital, Newcastle upon Tyme NHS Hospitals Foundation Trust, Newcastle upon Tyne, NE7 7DN, UK

conducting enzyme-linked immunosorbent assays (ELISA). Moreover, they are costly and labor-intensive, as patient blood must be drawn intravenously and transported to a centralized laboratory, where it is processed to derive serum or plasma and analyzed by trained personnel using specialized apparatus. The results are then relayed to a clinician before treatment can begin.[4,5] Given the time-sensitive nature of ACS diagnosis, this protracted workflow can be highly detrimental to patient outcomes while also resulting in prolonged hospital stays and unnecessary bed occupancy, which increases strain on healthcare systems, particularly in high-pressure environments like A&E departments.[6]

In the UK, approximately 700 000 individuals present to A&E each year with chest pain. Although over 75% are not experiencing ACS, many still undergo cardiac troponin (cTn) testing as part of the diagnostic workup. This widespread testing contributes to healthcare burdens and inefficiencies.[7–9] Consequently, there is a critical need for rapid, point-of-care (PoC) diagnostic alternatives to streamline this triaging process and provide timely, accurate results at the patient's location. Importantly, such technologies could facilitate ACS diagnosis in various settings, including ambulances, emergency rooms, and primary care clinics. One promising approach is the use of dermal interstitial fluid (ISF) for cardiac troponin I (cTnI) analysis. Human cTn consists of three subunits: troponin I (cTnI), troponin T (cTnT), and troponin C (cTnC). Among these, cTnI is a key protein released into the bloodstream when heart muscle cells are damaged, making it a highly specific, sensitive, and widely used biomarker for ACS diagnosis.[10,11] ISF surrounds tissue cells and contains a rich environment of biomolecules, making it a viable alternative to traditional blood sampling.[12–16] Despite its diagnostic promise, ISF has historically been underutilized due to the lack of non-invasive extraction methods. However, in recent years, minimally invasive techniques, such as microneedles and reverse iontophoresis, have been developed.[17,18] Unlike blood draws, which typically require invasive venipuncture and are often associated with patient discomfort and anxiety, these methods are less painful and traumatic, a significant benefit for the approximately 20% of adults with needle phobia.[19] The human body also contains roughly three times more ISF than blood, making it a more abundant biological matrix for sampling.[15] Furthermore, unlike serum or plasma generation, ISF sampling requires no processing, which further streamlines the diagnostic workflow and reduces time to diagnosis, thereby improving patient outcomes.[20]

Recent advancements in ISF sampling have led to the development of wearable devices capable of continuous biomarker monitoring.[21,22] While these devices have proven effective for detecting small molecules and ions, the detection of larger proteins, such as cTnI, remains a significant challenge.[16,23] Although ISF contains most of the same proteins as blood, it also exhibits distinct compositional differences due to selective filtration across the capillary endothelium. This filtration process allows smaller proteins and molecules (<70 kDa) to pass while restricting larger proteins (>70 kDa), potentially aiding in the detection of cTnI by reducing non-specific binding.[24–26] The transport of molecules similar in size to cTnI (24 kDa) from blood to ISF occurs through transcellular transport *via* vesicles and paracellular diffusion across endothelial junctions (Fig. 1A and B).[15,27,28]

To our knowledge, no previous studies have directly examined the variation in cTnI concentration between ISF and blood in humans. A recent preliminary study by Mirzajani *et al.* examined cTnI levels in serum and ISF extracted from rats ($n = 6$), reporting no significant difference in endogenous cTnI concentration between the two matrices.[29] While informative, these findings are limited by species differences. In the context of human ISF, initial studies proposed a logarithmic relationship between molecular weight and the abundance ratio of molecules in blood plasma *versus* ISF.[30] In more recent work, Oharazawa *et al.* reported a significant positive correlation between ISF levels from skin dialysate and blood plasma for 39 metabolites.[31] Similarly, Tran *et al.* performed an extensive comparative study on the prevalence of 407 proteins in ISF, plasma, and serum using a shotgun quantitative proteomic approach, confirming that ISF is highly similar to both plasma and serum, with variations at the quantitative level.[32] Interestingly, the literature demonstrates that numerous proteins of similar size to cTnI (24 ± 5 kDa) are more abundant in ISF than serum or plasma, by factors of 4.06–16.48 and 3.29–10.48, respectively (Table S3).[33] These variations in relative protein abundance may also be influenced by the time

Francesco Canfarotta

Francesco Canfarotta is Head of Chemistry at Tozaro, with 15 years' experience in polymer chemistry and nanotechnology applied to diagnostics (sensors & assays) and bioprocessing (separation). He was a Marie Curie Fellow and earned a PhD in polymer chemistry (nanotechnology) at the University of Leicester, developing molecularly imprinted polymer nanoparticles for diagnostic applications. He has co-authored 58 peer-reviewed publications (h-index 25) and is an inventor on multiple patents, contributing to the scientific and commercial growth of MIP-derived nanomaterials. He has recently completed an Executive MBA at the University of Cambridge. It is a pleasure to contribute as an invited author as Nanoscale Horizons marks an important anniversary of highlighting interdisciplinary nanoscale research. The journal's focus on discoveries that connect fundamental nano-enabled materials with practical impact aligns closely with our work on molecularly imprinted polymer nanoparticles for sensing and bioapplications. I hope this article reflects the inventive spirit that the journal champions and supports the community in translating next-generation nanotechnologies into real solutions. Congratulations to the editors, reviewers and authors for building such a vibrant forum.

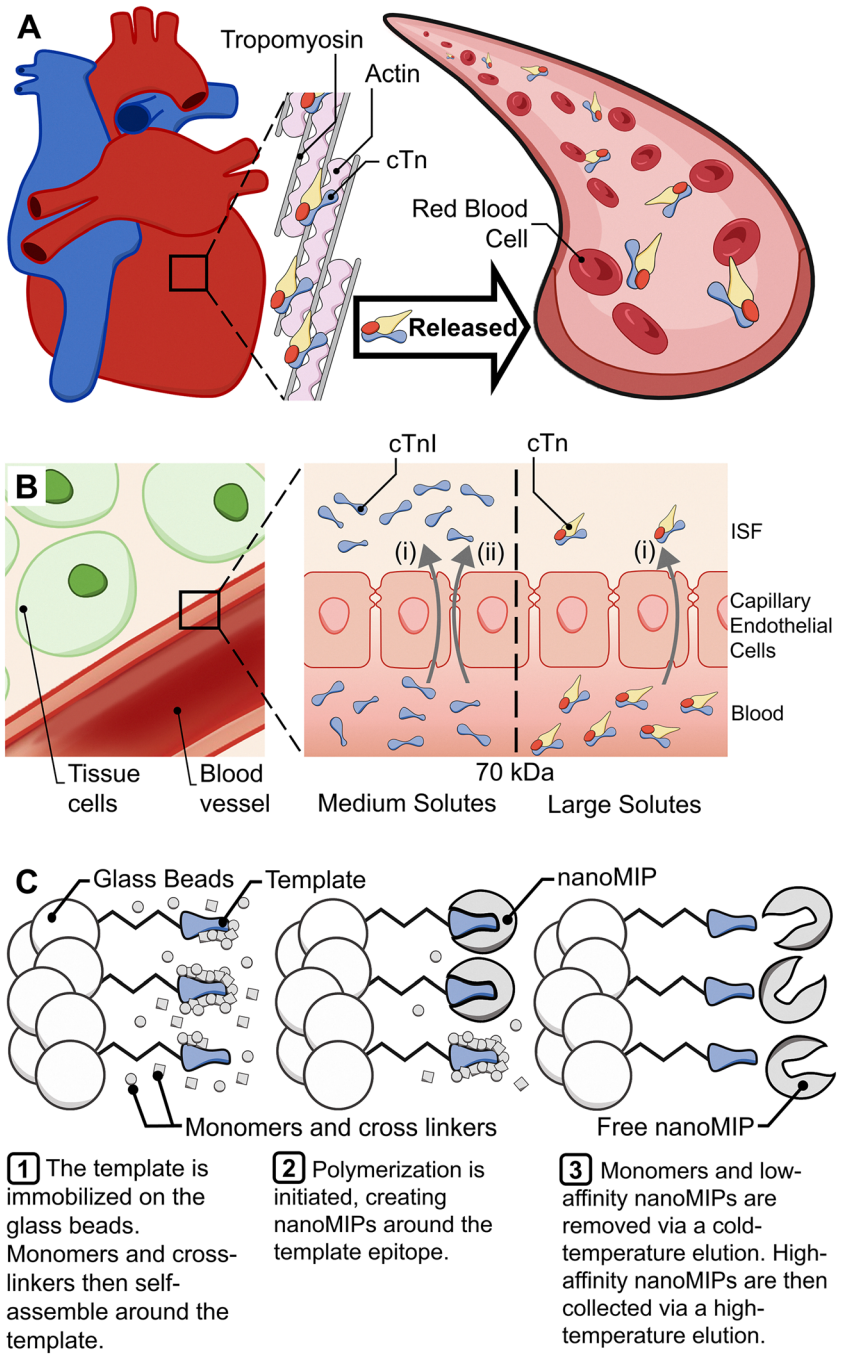

Fig. 1 (A) Schematic illustrating the release of the cTn complex from heart muscle into the bloodstream during ACS. (B) Schematic depicting the expected movement of cTn(I) molecules across the capillary endothelial cells, based on the known size-dependent behavior of the capillary interface. Analyte transfer across this interface can occur *via* two routes: (i) paracellular diffusion between cells *via* interendothelial junctions or (ii) transcellular transport through the cell *via* vesicles. (C) Schematic outlining the solid-phase synthesis of nanoMIPs using a small epitope of cTnI as the template.

required for proteins to diffuse from blood to ISF, or by their pre-existing presence in ISF at higher levels than in blood.[15,34] This "lag time" is well documented in glucose sensing, where ISF concentrations take several minutes to align with plasma levels.[16] Nevertheless, the relationship between ISF and plasma concentrations remains complex and depends on the specific biomarker, extraction methods, and patient characteristics, as highlighted by conflicting reports across the literature.[15,16,26,35,36]

Most ISF extraction methods suffer from issues related to sample extraction rates and total extractable volume, which limit the practical use of ISF as a diagnostic matrix. For instance, many microneedle-based platforms have been shown to extract a maximum of 16 μL over 2 h.[15,37] Conversely, methods that yield higher volumes, such as blister suction extraction (~500 μL in 1 h) and *in vivo* microdialysis, are invasive.[37,38] The technology developed by KIFFIK Biomedical, Inc. (RI, United States) overcomes these

limitations by enabling non-invasive, high-volume ISF extraction. It employs a two-step process in which non-invasive electrodes induce electroporation to generate microchannels through the epidermis. This is followed by the activation of a small negative pressure pump, which facilitates ISF extraction at a rate of up to 1 mL h^{-1}, significantly greater than that of other common methods.[37] This increased yield, combined with its non-invasive nature, positions the technology as a promising alternative for ISF-based diagnostics.

In this study, we present a novel approach that combines molecularly imprinted polymer nanoparticles (nanoMIPs) as artificial recognition elements with the heat-transfer method (HTM) to create a rapid and cost-effective platform for detecting cTnI in ISF.[39] HTM offers several advantages over conventional detection methods, such as electrochemical and optical techniques. Notably, the baseline signal in HTM exhibits high stability, eliminating the need for electrode pre-treatment, stabilization protocols, or the incorporation of nanomaterials to enhance the signal. Additionally, HTM does not require redox probes or molecular labels, simplifying the measurement protocol. These features contribute to improved reproducibility and robustness across measurements, particularly in complex biological matrices. NanoMIPs match the binding affinity of antibodies while offering crucial advantages, including exceptional environmental stability, extended shelf life (lasting years), and no requirement for refrigeration.[40,41] By utilizing high-affinity nanoMIPs for cTnI detection fabricated *via* epitope imprinting and solid-phase synthesis, previously shown to achieve excellent sensitivity and selectivity, we provide a clinically practical alternative for cTnI sensing (Fig. 1C).[42–44] Functionalized onto screen-printed electrodes (SPEs) within a microfluidic-based system, these nanoMIPs enable precise and reliable quantification of cTnI levels, ensuring accessibility to rapid, accurate cardiac biomarker assessment in clinical settings.[45,46] Therefore, this novel sensor platform holds substantial potential for enabling early detection of cardiac events, streamlining diagnostic workflows, and broadening access to essential clinical testing.

This study is the first to report the detection of cTnI in human ISF, underscoring the potential of ISF sampling as a more efficient and patient-friendly alternative to traditional blood tests for ACS diagnosis. By conducting measurements in human serum, plasma, and ISF, we demonstrate that ISF can be a highly effective diagnostic medium for ACS. This capability positions ISF sampling as a transformative approach for frequent and convenient biomarker monitoring, which could greatly reduce diagnostic times, improve patient outcomes, and ease the strain on healthcare systems. Although this study is focused on ACS, the findings have broader implications for diagnosing and monitoring a wide range of health conditions, highlighting ISF's potential as a versatile and accessible diagnostic tool.

2. Experimental section

2.1. Materials

4-Aminobenzoic acid (4-ABA, 99%, Cat. No. 11359429), 1-ethyl-3-(3-dimethylaminopropyl) carbodiimide (EDC, Premium Grade, Cat. No. 15285763), hydrochloric acid (HCl, 37%, Cat. No. 10053023), *N*-hydroxysuccinimide (NHS, Cat. No. 10772155), phosphate buffered saline (PBS) tablets (Cat. No. 10209252), and sodium nitrate (98+%, Cat. No. 11429443) were purchased from Fisher Scientific (Loughborough, UK). cTnI from the human heart (Cat. No. T9924), human plasma (Cat. No. P9523), human serum (Cat. No. H4522), potassium chloride (≥99.0%, Cat. No. P4504), potassium ferricyanide(III) (99%, Cat. No. 702587), potassium hexacyanoferrate(II) trihydrate (≥99.5%, Cat. No. 60279), and sodium hydroxide (≥97%, Cat. No. 221465) were purchased from Sigma-Aldrich (Gillingham, UK). Human interstitial fluid (ISF) samples were provided by KIFFIK Biomedical (RI, USA) and collected at their site using the company's proprietary electroporation-based device. Deionized (DI) water with a resistivity of 18.2 MΩ cm was used throughout.

The human serum and plasma were prepared from pooled human blood collected from healthy adult male donors, as specified by Sigma-Aldrich. The human blood samples were purchased from Sigma-Aldrich for commercial purposes. For detection experiments, a stock solution of cTnI (10 ng mL^{-1} in PBS) was prepared, aliquoted, and stored at −20 °C. A fresh aliquot was used for each set of experiments to prevent protein degradation caused by repeated freeze–thaw cycles. All aliquots used in the main study were stored for less than three months. Supplementary experiments (see SI for details) employed cTnI from the same supplier (Cat. No. T9924), stored in aliquots at −20 °C for two years.

2.2. ISF sample preparation

KIFFIK Biomedical has developed a patented (US20120041288A1), non-invasive wearable device designed to extract and collect pure, native ISF. The device utilizes electroporation to apply pulsed and non-pulsed voltage to the skin, creating numerous micro-sized pores in the stratum corneum. A negative pressure is then applied *via* a pump to continuously extract ISF.[47] The device is currently undergoing regulatory approval for the FDA (United States), CA marking (UK), and CE marking (European Union). ISF extraction rates vary between individuals due to physiological factors such as skin thickness, hydration status, skin temperature, and perfusion pressure. The device can extract up to 1 mL of ISF per hour, a significantly greater volume compared to microneedle or microdialysis-based methods.[37] ISF samples were collected from healthy male volunteers (n = 2), pooled, and stored at −20 °C until use.

2.3. NanoMIP synthesis and characterization

NanoMIPs were synthesized using a solid-phase approach, in which glass beads (70–100 μm) were first activated with 2 M sodium hydroxide and subsequently functionalized with an amino silane to generate free surface amine groups. The target epitope used for the cTnI recognition was a 10-amino-acid sequence located within the stable chain region of cTnI (AA: 34–126). This specific epitope was selected using computational approaches to visualize the 3D structure of the protein and evaluate its accessibility. The epitope was immobilized onto the amine-derivatized glass beads *via* succinimidyl iodoacetate

coupling. NanoMIPs were then prepared according to a proprietary modification of the protocol described by Canfarotta *et al.*, involving the radical polymerization of functional and cross-linker monomers at room temperature for 1 h (Fig. 1C).[43] Unreacted monomers and low-affinity nanoMIPs were removed through low-temperature elution (20 °C), after which high-affinity nanoMIPs were collected using high-temperature elution (60 °C).

The hydrodynamic diameter of the nanoMIPs was measured using dynamic light scattering (DLS) on a Malvern Zetasizer Nano ZS (Malvern, UK) at 25 ± 0.1 °C, with a scattering angle of 173° and laser wavelength of 632.8 nm. NanoMIP morphology was examined using atomic force microscopy (AFM) conducted in air using a Bruker Nanowizard V (CA, USA) operating in quantitative imaging mode. All images (height and adhesion contrast) were obtained using Bruker SCANASYST-AIR probes with a nominal tip radius of 2 nm, spring constant of 0.4 N m^{-1}, and cantilever length of 115 μm. Before imaging, nanoMIP solutions (0.631 mg mL^{-1}) were drop-cast onto freshly cleaved mica substrates (Agar Scientific, Rotherham, UK) and allowed to dry overnight under ambient conditions. All AFM data analysis was performed using the freeware Gwyddion.

2.4. Electrode functionalization and characterization

The SPEs were manufactured to meet specific experimental requirements (see SI for details). NanoMIPs were immobilized onto SPEs *via* electrografting followed by EDC/NHS coupling (Fig. 2A).[44,45] Briefly, the SPE was submerged in a solution of 2 mM 4-ABA and 2 mM sodium nitrate in 0.5 M aqueous HCl, and cyclic voltammetry was employed to electrograft 4-ABA onto the electrode surface. To activate the carboxyl groups, a solution of 100 mM EDC and 20 mM NHS in PBS buffer (pH 5) was drop-cast (8 μL) onto the SPE and left for 1 h. A nanoMIP solution was then drop-cast onto the SPE (8 μL), facilitating covalent immobilization *via* amide bond formation. The SPE was left for 8 h before being rinsed with DI water. Electrochemical impedance spectroscopy (EIS) measurements were conducted using a PalmSens Sensit Smart (Houten, The Netherlands) across a fixed frequency range of 0.1 Hz to 100 kHz to confirm nanoMIP immobilization on the SPEs. Measurements were performed at each stage of the immobilization protocol in a PBS solution containing 1 mM potassium ferricyanide(III), 1 mM potassium hexacyanoferrate(II) trihydrate, and 0.1 M KCl. Charge-transfer resistance was extracted by fitting the impedance data to an equivalent circuit model, such as the Randles circuit.

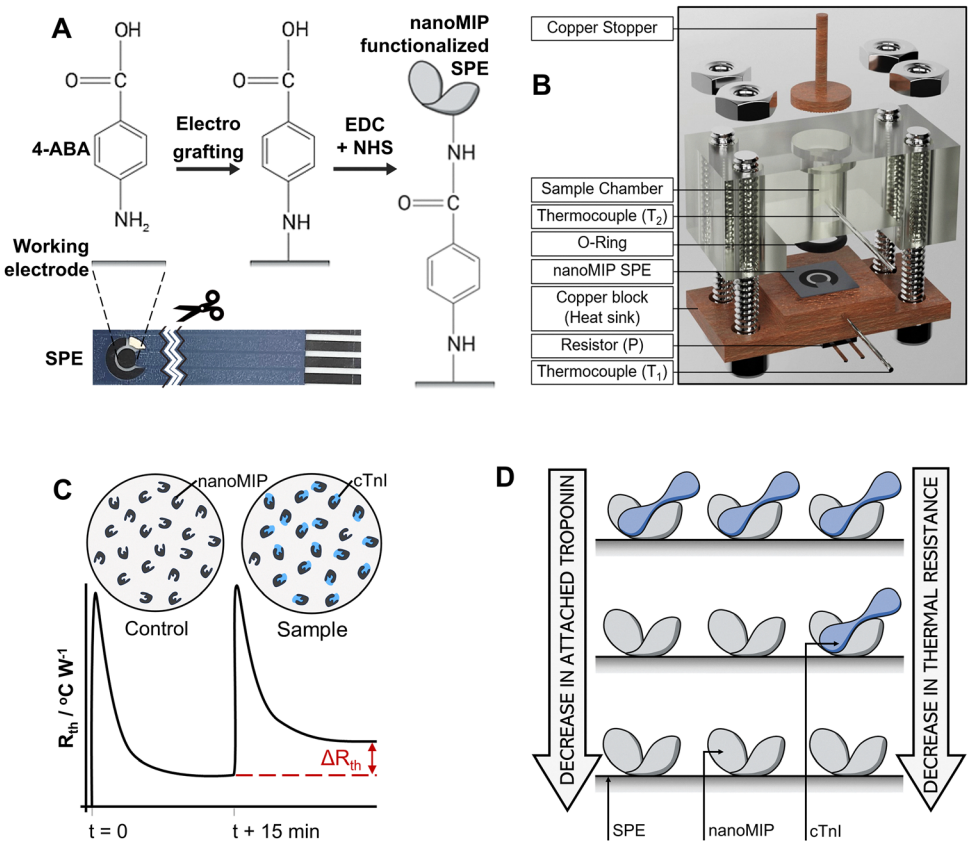

Fig. 2 (A) Schematic illustrating the covalent immobilization of cTnI nanoMIPs onto the working electrode of a SPE. (B) Schematic of the measurement cell setup for cTnI detection using the HTM. (C) Example of a typical response for the HTM: a control sample with no cTnI is added to the cell, establishing the system's baseline R_{th} value. After removing the control sample, a spiked sample of known cTnI concentration is added. Increased cTnI levels result in greater binding to the nanoMIPs, increasing the R_{th}. The difference between the two R_{th} values provides the ΔR_{th}. (D) Schematic showing how cTnI binding to nanoMIPs increases R_{th}.

2.5. Thermal measurements

The microfluidic cell used for thermal experiments is shown in Fig. 2B, where the nanoMIP-functionalized SPE was centered on a copper block and sealed with a rubber O-ring to prevent leakage.[39] The temperature was recorded at two points: the copper block (T_1), which was fixed at 37.00 ± 0.02 °C, and in the sample chamber (T_2), located 4 mm above the SPE. The cell was connected to a heat transfer device that monitored temperature changes and controlled T_1 *via* an optimized proportional-integral-derivative (PID) controller (P = 1, I = 14, D = 0.3), as described by van Grinsven *et al.*[48] Both temperatures and the power (P) supplied to the copper block were recorded every second to calculate the thermal resistance of the system (R_{th}) using eqn (1).[49]

$$R_{th} = \frac{T_1 - T_2}{P} \quad (1)$$

The HTM operates on the principle of thermal resistance; as the target molecule (*e.g.*, cTnI) binds to the nanoMIPs, it reduces heat transfer from the copper block to the sample chamber, resulting in a lower T_2 and an increased R_{th} (Fig. 2C and D). For preliminary HTM measurements, a baseline R_{th} was established by measuring two control samples (*e.g.*, native ISF, serum, or plasma), followed by a spiked solution with a known cTnI concentration. However, the results were highly consistent, allowing for calibration; therefore, measurements of only one control sample were required, which reduced the measurement time to 15–20 min. Each test solution was added to the chamber using a pipette (120 μL), covered with a copper lid to minimize heat exchange, and allowed to stabilize. After stabilization, 100 data points were collected, from which an average R_{th} value was calculated for each concentration. The solution was then removed with a pipette, and the next concentration was added. A single nanoMIP-functionalized SPE was used for each sample, which included additions of multiple cTnI concentrations. This process was repeated to determine ΔR_{th} between baseline and spiked samples for all matrices. Data from triplicate measurements were used to calculate the limit of detection (LoD) values with a 95% confidence interval, employing the three-sigma method (LoD = $3.3\sigma/S$), where σ represents the standard deviation of the baseline signal and S is the slope of the dose–response curve.

The method offers several features that make it highly suitable for PoC diagnosis. First, the integration of nanoMIPs for specific molecular recognition ensures excellent selectivity for cTnI, which is essential for clinical relevance. The compact HTM setup relies on straightforward thermal resistance measurements, eliminating the need for complex equipment or reagents. The total time from sample loading to result is approximately 15–20 min, typically comprising ~10 min for thermal stabilization followed by up to 10 min for a cTnI measurement. The ΔR_{th} value is calculated by averaging 100 data points from the concentration baseline and subtracting this from the control baseline. At present, this calculation is performed manually; however, in future work, we aim to implement an automated calibration curve to directly convert ΔR_{th} into cTnI concentration, with the results displayed *via* a simple digital readout. The short assay time and minimal sample volume (120 μL) further enhance the sensor's utility in scenarios where rapid and minimally invasive testing is critical. This novel diagnostic approach addresses the urgency of ACS diagnosis during the "golden hour," potentially reducing delays associated with centralized laboratory processing and thereby improving patient outcomes.

3. Results and discussion

3.1. NanoMIP characterization

DLS analysis revealed that the nanoMIPs had a hydrodynamic diameter of 89 nm, with a low polydispersity index of 0.22 (Fig. 3A). Similarly, AFM images revealed an average nanoMIP diameter of 77.2 ± 14.2 nm (Fig. 3B–D). This variation in nanoMIP size between the scattering and microscopy methods can be attributed to the different conditions under which the analyses were performed: DLS measurements were conducted in DI water, while AFM was carried out in a dry state, indicating moderate swelling of the nanoMIPs, a typical characteristic of polymer nanoparticles. The AFM images also demonstrate the predominantly spherical morphology of the nanoMIPs, as exemplified in Fig. 3E, which shows a cross-sectional profile plot of an individual nanoMIP fitted to a spherical cap. These findings confirm that the nanoMIPs exhibit uniform morphology with a relatively monodisperse size distribution, which is crucial for ensuring reproducible sensor performance.[50] The immobilization of nanoMIPs onto SPEs was evaluated using EIS. The resulting Nyquist plots display a progressive increase in charge-transfer resistance at each preparation step (from 4.3 to 33.84 kΩ), indicating successful immobilization of the non-electroactive nanoMIPs (Fig. 3F and Table S1).

3.2. Thermal sensing of cTnI in ISF

Preliminary experiments were conducted to confirm that the nanoMIP-based thermal sensor could effectively operate in ISF and detect cTnI within this complex biological matrix, which contains numerous small molecules and proteins.[15] Baseline R_{th} measurements were taken from two native ISF samples, which served as controls, followed by ISF spiked with a relatively high cTnI concentration (100 pg mL^{-1}), representing levels associated with myocardial injury. The control measurements showed no statistically significant difference in R_{th}, while the cTnI-spiked ISF exhibited a considerably higher R_{th} value (Fig. 4A). The corresponding dose–response plot in Fig. 4B includes a red dashed 3σ line, representing three times the baseline σ of the first control sample. The R_{th} of the 100 pg mL^{-1} cTnI sample is well above this detection threshold, confirming that the nanoMIP sensor can reliably detect physiological levels of cTnI in human ISF in real-time.

To effectively evaluate the nanoMIP-HTM approach for cTnI sensing in ISF, a dynamic concentration range was required. A blood concentration of 40 pg mL^{-1} represents the 99th percentile in a healthy population,[51] with levels exceeding this threshold strongly indicating cardiac injury and necessitating further investigation. Specifically, cTnI concentrations equal to or

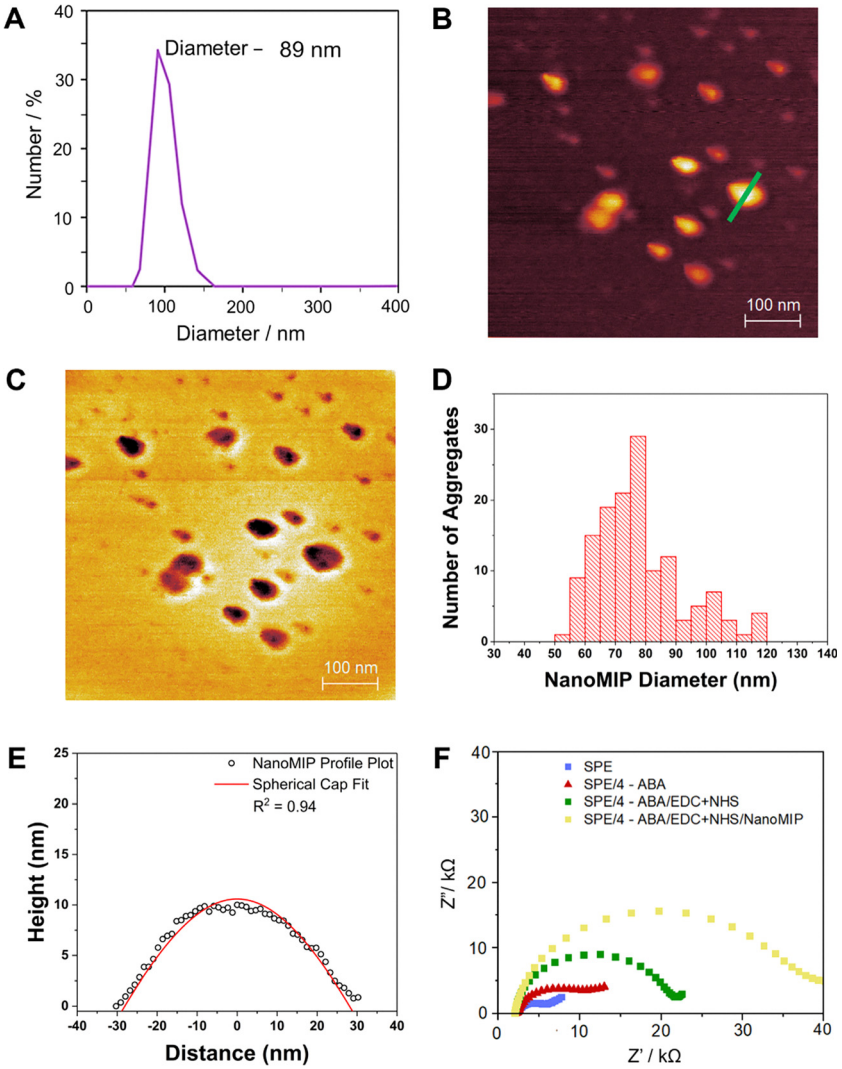

Fig. 3 (A) DLS spectrum presenting the size distribution of cTnI nanoMIPs. (B) AFM height image of cTnI nanoMIPs on a freshly cleaved mica substrate. (C) Corresponding AFM adhesion image. (D) Histogram showing the distribution of nanoMIP diameters from 140 measurements. (E) Cross-sectional profile plot of an immobilized nanoMIP, represented by the green line in panel (B), fitted to a spherical cap (R^2 = 0.94). (F) Nyquist plot overlaying EIS measurements of a blank SPE, 4-ABA electrografted onto the SPE, carboxyl group activation, and covalent coupling of nanoMIPs.

greater than 400 pg mL^{-1} typically signify an ACS, requiring urgent clinical intervention.[51] However, values between these thresholds require serial measurements and careful clinical interpretation, as they may indicate cardiac injury without definitively confirming ACS. To comprehensively cover the physiologically relevant range, a concentration span from 0.1 to 1000 pg mL^{-1} in human ISF was employed, ensuring sensitivity to both subclinical and critical cTnI levels. This supports the sensor's utility for real-time PoC applications while accounting for the uncertain dynamics of cTnI transport into ISF. The exact relationship between cTnI concentrations in human blood and ISF remains speculative, as no studies have directly examined their variation, adding uncertainty to this correlation.

The findings demonstrate that the thermal response increased progressively with each increment in cTnI concentration, spanning four orders of magnitude (1 to 1000 pg mL^{-1}, ****, $p < 0.0001$) and encompassing the physiologically relevant range of cTnI in blood, as well as any potential variation in ISF (Fig. 4C; see Table S4 for data). The nanoMIP-based sensor exhibited an excellent LoD of 1.85 ± 0.32 pg mL^{-1} in ISF, which is significantly lower than the 99th percentile value for cTnI in healthy individuals' blood (40 pg mL^{-1}).[51] Notably, this LoD and the corresponding sensitivity (0.24 ± 0.04 pg mL^{-1}) are substantially lower than those reported for commercial "gold-standard" ELISAs, which exhibit 10% trimmed mean LoD and sensitivity values of 31.8 and 34.1 pg mL^{-1}, respectively, for measurements in serum (Table 1).[44,52,53] Some ELISAs report LoD and sensitivity values as high as 391 and 240 pg mL^{-1}, respectively, which is approximately 2.5 orders of magnitude higher than those achieved with our sensor.

Unlike many ELISA methods that require sample dilution (typically 2-fold), our sensor operates directly with undiluted ISF, serum, and plasma, thereby preserving analyte concentrations and simplifying the measurement protocol. Additionally,

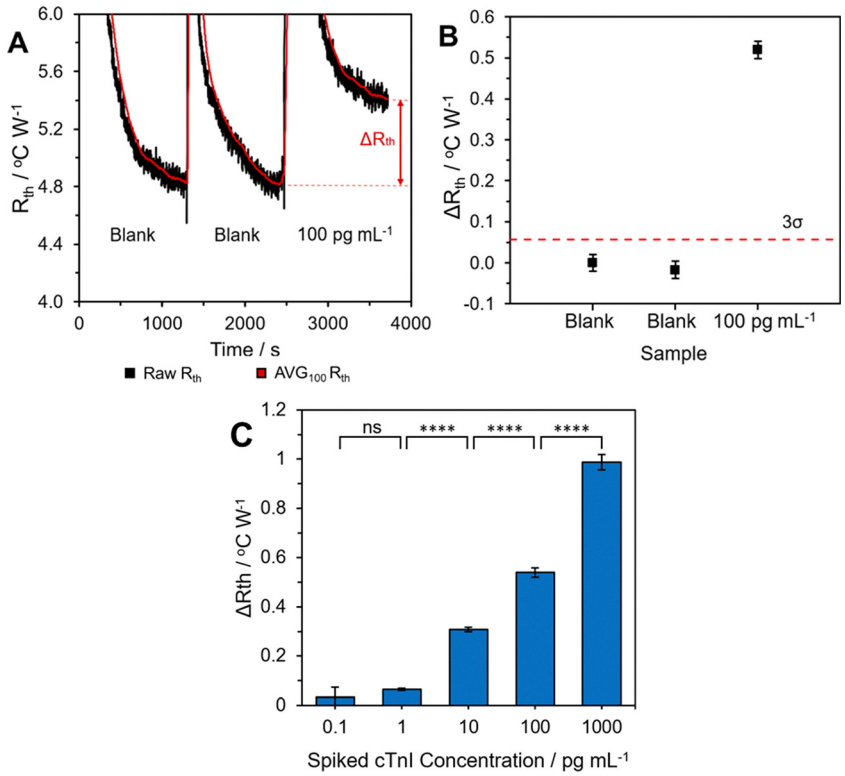

Fig. 4 (A) Typical raw (black) HTM data plot (R_{th} *vs.* time) with a moving average overlay (red), demonstrating the clear thermal response to the presence of cTnI. (B) Corresponding ΔR_{th} plot. (C) Thermal detection of various cTnI concentrations (0.1–1000 pg mL^{-1}) in spiked human ISF samples.

Table 1 Comparison of commercially available, gold-standard ELISAs for cTnI detection. Further comparisons of LoDs can be found in the works of Tada *et al.*,[54] Wu *et al.*,[55] and Brandmeier *et al.*[56] T mean = 10% trimmed mean

Brand name	Sensitivity/ pg mL^{-1}	LoD/pg mL^{-1}	Sample dilution factor	Technology-reaction-detection	Procedure time
ThermoFisher Scientific –Invitrogen (EHTNNI3)	100	0.38	2-fold	ELISA-sandwich-colorimetric	4 h 45 min
ThermoFisher Scientific – Invitrogen (A46074)	<0.3	0.32	10-fold	Proximity-based immunoassay	2 h
Antibodies.com (A77930)	7.5	12.5	2-fold	ELISA-sandwich-colorimetric	4 h
Sigma-Aldrich (RAB0634)	100	125	2-fold	ELISA-sandwich-colorimetric	4 h 45 min
ELK Biotechnology (ELK9080)	9.53	31.3	No dilution	ELISA-sandwich-colorimetric	3 h 30 min
Abcam (ab200016)	4.4	31.3	No dilution	ELISA-sandwich-colorimetric	1 h 30 min
Abcam (ab229404)	17	20	4-fold	ELISA-sandwich-fluorescent	1 h 30 min
Abbexa (abx252868)	240	391	—	ELISA-sandwich-colorimetric	3 h 20 min
Millipore (03-0254-00)	0.35	2	2-fold	Single molecule counting	1 h 40 min
Averages	53.2 (mean) 34.1 (T mean)	68.6 (mean) 31.8 (T mean)	—	—	3 h 15 min
Current work	0.24	1.85 (ISF) 1.80 (serum) 1.78 (plasma)	No dilution	NanoMIP-thermal	15–20 min

the turnaround time of our method (15–20 min) is significantly shorter than the ELISA average of 3 h 15 min, with some assays requiring more than 4 h. Collectively, these results demonstrate that the nanoMIP-based thermal sensor can reliably detect varying concentrations of spiked cTnI in ISF samples with excellent sensitivity, in addition to offering rapid turnaround time and minimal sample preparation. Moreover, the device's hardware is low-cost compared to commercial alternatives, which typically require microplate readers for analysis. The HTM components and Kiffik's extraction device cost approximately £1500 and £1000, respectively, although neither is currently commercially available. Following this initial investment of around £2500, each disposable nanoMIP-functionalized SPE costs approximately £0.25, making the device extremely low-cost to operate. These advantages highlight the sensor's potential for integration into current clinical diagnostic pathways, providing a highly sensitive PoC alternative for cTnI detection.

Notably, the LoD of our nanoMIP-based sensor in ISF is comparable, or superior to, the most sensitive cTnI tests reported in recent literature using PBS or blood derivatives (Table 2).[57–61] For instance, Han *et al.* developed a paper-based vertical flow immunoassay with an excellent LoD of 0.2 pg mL^{-1} in serum,

Table 2 Comparison of PoC devices for cTnI detection, including both commercially available systems and the most promising recent methods reported in the literature. EDTA = ethylenediaminetetraacetic acid. Hep = heparinized. WB = whole blood. An expanded version of this table with additional data is available in Table S5

Brand name/study	Technology	Specimen	LoD/pg mL^{-1}	Sensitivity/ pg mL^{-1}	Time/ min
Fu *et al.*[62]	Electrochemical paper-based device, EIS immunoassay	Undiluted plasma	4.6	—	46
Han *et al.*[63]	Paper-based vertical flow immunoassay	Undiluted serum	0.2	<1	15
Campu *et al.*[64]	Thermo-plasmonic SPR and surface-enhanced Raman spectroscopy	Undiluted plasma	1.6	—	<5
Lee *et al.*[58]	Electrochemical immunosensor	Undiluted WB	6.86	—	5
Choudhary and Altintas[42]	cTnI nanoMIP-SPR	PBS	520	—	10
hs-cTnI-SPINCHIP[65]	Benchtop fluorescence immunoassay	WB or Li Hep plamsa	1.1	—	10
LSI Medicine Corporation PATHFAST[59,60,66]	Benchtop chemiluminescent analyzer	Na Hep, Li Hep, or EDTA WB or plasma	2.9	20	17
Abbott i-STAT[59,62,66]	Handheld two-site immunometric assay	Na and Li Hep WB or plasma	20	25	10
Siemens Atellica VTLi[59,60]	Immunoassay analyzer Magnotech®	Li Hep WB or plasma	1.6 (WB) 1.2 (plasma)	—	8
QuidelOrtho TriageTrue[59,60]	Hs-TnI fluorescence immunoassay	EDTA WB or plasma	1.5–1.9 (WB) 0.7–1.6 (plasma)	—	<20
Response Biomedical RAMP[59,60]	Benchtop lateral flow immunoassay	EDTA WB	30	200	8–15
Current work	cTnI nanoMIP-thermal	ISF, serum, plasma	1.85 (ISF) 1.80 (serum) 1.78 (plasma)	0.24	15–20

while Campu *et al.* employed thermo-plasmonic surface plasmon resonance (SPR) to achieve 1.6 pg mL^{-1} in plasma. Fu *et al.* and Lee *et al.* utilized EIS to detect cTnI in plasma and whole blood, achieving LoDs of 4.6 and 6.86 pg mL^{-1}, respectively. Although these platforms demonstrate high sensitivity in undiluted biological matrices, they rely on antibodies as recognition elements, which suffer from poor environmental stability, resulting in limited shelf life and stringent storage conditions for the devices. In contrast, Choudhary and Altintas employed nanoMIPs in a SPR-based sensor, but their LoD was 520 pg mL^{-1}, and measurements were only conducted in PBS.[42] This significantly limits diagnostic relevance, as PBS lacks the complexity of clinical biofluids and does not account for non-specific binding effects. Our sensor, by comparison, was validated in ISF, a complex biofluid containing a wide array of non-specific binders (*e.g.*, proteins, electrolytes, metabolites).[14] This markedly enhances the clinical relevance of our device, ensuring that measurements are not only sensitive but also robust against the complexities of real patient samples. These results demonstrate the nanoMIP-based sensor's ability to reliably detect cTnI in complex matrices with numerous interferents. Moreover, the assay time was only 15–20 min, with potential for further reduction, and the required sample volume was just 120 μL, which is compatible with some current ISF extraction technologies (*e.g.*, Kiffik's device).

When benchmarked against commercially available PoC devices, our nanoMIP-based sensor also demonstrates clear advantages, particularly in terms of LoD and operational robustness. The mean LoD across commercial PoC devices, including those listed in Table S4, is 10.7 pg mL^{-1}, substantially higher than the LoD achieved by our sensor (1.85 ± 0.32 pg mL^{-1}). Systems such as the Siemens Atellica VTLi, SPINCHIP, LSI PATHFAST, and QuidelOrtho TriageTrue report low LoDs ranging from 0.7 to 2.9 pg mL^{-1} in plasma or whole blood. However, other widely used platforms, including the Abbott i-STAT and Response Biomedical RAMP, exhibit markedly higher LoDs of 20 and 30 pg mL^{-1}, respectively. Moreover, all commercial PoC devices rely on antibodies as recognition elements, necessitating refrigerated storage (3–5 °C) and limiting shelf life. In contrast, nanoMIPs offer excellent environmental stability and eliminate cold-chain requirements. The assay time of our method (15–20 min) is comparable to that of commercial devices (mean = 13.7 min), with potential for further reduction. Overall, these findings demonstrate that our sensor compares favorably with existing PoC platforms and represents the first demonstration of highly sensitive and selective cTnI detection in human ISF using MIP technology, positioning it as a promising tool for PoC diagnosis of ACS.

The current study does not include measurements of endogenous cTnI in ISF; however, our sensor achieved a LoD of 1.85 ± 0.32 pg mL^{-1}, which is substantially lower than the 99th percentile threshold in blood (40 pg mL^{-1}), indicating sensitivity across the full physiological range.[51] While the direct correlation between cTnI concentrations in ISF and serum/plasma remains unconfirmed, existing literature suggests minimal dilution for proteins of similar size. For example, comparative proteomic studies have shown that proteins within the 24 ± 5 kDa range, similar to cTnI, are often present in ISF at comparable or even higher concentrations than in plasma (Table S3).[33] Additionally, Mirzajani *et al.* reported no statistically significant difference between endogenous cTnI levels in rat ISF (mean ≈ 3 pg mL^{-1}) and serum (mean ≈ 6.5 pg mL^{-1}).[29] These findings strongly suggest that, given the high sensitivity of our sensor across several orders of magnitude, it is capable of detecting endogenous cTnI in human ISF.

To further investigate the molecular recognition mechanism of the nanoMIPs, sensor performance was compared using fresh (1-day-old) and degraded (2-year-old) cTnI samples. These comparisons, detailed in the SI, provide insight into how

conformational changes and truncation of the cTnI molecule influence binding to the nanoMIP cavities. The results show that, while degradation reduced binding affinity, the nanoMIPs retained favorable recognition capabilities across a wide, physiologically relevant range (Fig. S2). This is a significant finding, as it is essential that diagnostic techniques can detect both intact and degraded forms of cTnI, given that cTnI can undergo varying degrees of proteolytic degradation depending on the severity of ischemia.[67]

3.3. Comparison with serum and plasma

The potential of ISF as a blood proxy for diagnostics is evident; however, few studies have evaluated the performance of novel sensors across various biological matrices, such as ISF, plasma, and serum, which hinders translational progress toward clinical integration. Therefore, to ensure the robustness of our nanoMIP-based sensor, we repeated thermal measurements using cTnI-spiked serum and plasma to assess whether the presence of different biological molecules in these fluids affected cTnI detection. In clinical practice, blood draws are the standard method for obtaining a snapshot of cardiac biomarker levels *via* the analysis of blood serum or plasma.[66] Serum and plasma have similar compositions, with total protein concentrations of 60–80 mg mL^{-1} and viscosities ranging from 1.4 to 1.8 mPa s; their primary distinction is the absence of clotting factors in serum.[68–71] In contrast, ISF viscosity values reported in the literature range from 1.3 to 3.5 mPa s. Moreover, its total protein concentration is only 50–60% of that in serum or plasma, as ISF has naturally reduced concentrations of large proteins, such as immunoglobulins (>150 kDa), fibrinogen (340 kDa), and albumin (66 kDa).[15,68,72–75] Despite these compositional differences, serum, plasma, and ISF share many common proteins. For instance, a study by Tran *et al.* identified 3270 proteins (93.3%) shared across all three matrices.[32] Additionally, comparative analyses by Sjöbom *et al.* and Samant *et al.* revealed 86% and 84–94% protein commonality between plasma and ISF, respectively.[26,76]

The nanoMIP-based sensor exhibited a similar thermal response to cTnI-spiked ISF, serum, and plasma at concentrations ranging from 1 to 1000 pg mL^{-1}. There was a high degree of statistical significance between each concentration (****; $p < 0.0001$) and minimal or no statistical significance within each concentration (*; $p \leq 0.05$, ns; $p \geq 0.05$). These results confirm that the nanoMIP-HTM methodology can accurately detect varying cTnI concentrations irrespective of other biological molecules present in the biofluid, suggesting that the nanoMIPs successfully minimized non-specific binding due to their tailored polymeric cavities specific to a small epitope of the cTnI protein (Fig. 5A).[77,78] This is further supported by the dose–response curve in Fig. 5B, which shows a clear logarithmic trend typical of traditional ELISA-based testing methodologies for cTnI quantification. The high confidence present in these trends indicates that our nanoMIP-based sensor maintains its high affinity for cTnI across a wide concentration range, despite the complexity of the biological matrices. The LoD values for cTnI detection in serum and plasma were 1.80 ± 0.22 and 1.78 ± 0.28 pg mL^{-1}, respectively, which are not statistically different from the value obtained in ISF (1.85 ± 0.32 pg mL^{-1}). The low statistical significance within each concentration across the three matrices suggests that ISF has strong potential to be utilized as a non-invasive biofluid for ACS diagnosis.[15,79]

The comparative results highlight the excellent versatility and sensitivity of the nanoMIP-based thermal sensor, as it exhibits lower LoD values than most gold-standard immunoassays (0.32–391 pg mL^{-1}) in three diagnostically relevant sample fluids (Table 1 and Table S5).[54–56] As nanoMIPs can be easily tailored to virtually any target by changing the template molecule/epitope, the developed technology could enable sensitive detection of a wide range of biomarkers in various sample media. Selectivity testing was not directly performed in ISF due to practical constraints. However, in a previous study, we rigorously evaluated cTnI nanoMIP selectivity in buffered solutions spiked with cTnT, albumin, and glucose, yielding results that demonstrated excellent selectivity for cTnI.[44] Further validation in ISF is required and represents a limitation of the current study, which will be addressed in future work. Despite this, the thermal measurements indicate that non-specific binding in the extracted ISF is comparable to that in serum and plasma, allowing for accurate and consistent detection across these biofluids. This showcases the use of ISF as a viable blood proxy in ACS diagnosis, particularly

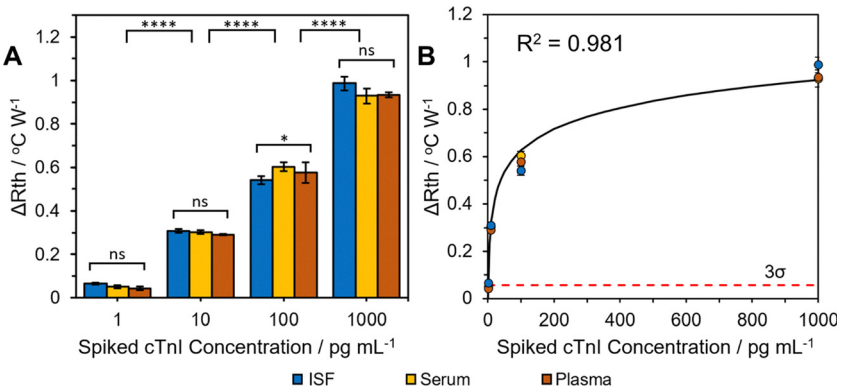

Fig. 5 (A) Comparison of the thermal response for cTnI detection in human ISF, serum, and plasma at different concentrations (1–1000 pg mL^{-1}). (B) Corresponding logarithmic dose–response curve for the three sample fluids.

with the development of wearable devices capable of extracting biomarker-rich ISF in a minimally invasive manner (*e.g.*, Kiffik's device), thereby reducing patient discomfort, pain, and anxiety associated with repeated blood draws.[12,16,47] Additionally, wearable ISF sampling technologies could significantly contribute to the drive toward personalized healthcare by enabling continuous, real-time health monitoring without disrupting patients' daily routines or increasing infection risk.

Importantly, future clinical validation must account for variability in ISF extraction and biomarker content arising from factors such as skin site location, hydration status, temperature, and inflammatory responses. Although efforts were made to minimize ISF variability in the current study, the ISF samples were pooled before analysis to enable a consistent matrix for each measurement. Human skin is anatomically heterogeneous, exhibiting regional differences in dermal and epidermal thickness, sweat gland and hair follicle density, and mechanical properties.[80] This heterogeneity can affect both the volume and rate of ISF extraction, as well as the composition of the extracted fluid. For instance, Kawakatsu *et al.* demonstrated that continuous glucose monitoring readings differed significantly between the right and left arms (n = 46), suggesting that even minor anatomical shifts can influence ISF-derived measurements.[81] In the present study, ISF samples were collected from the same position on the left upper arm of two healthy adult male volunteers, minimizing any influence from skin site heterogeneity. Additionally, factors such as age and hydration status can significantly impact skin biomechanics, while skin temperature has been shown to enhance permeability by opening hair pores and activating sweat glands, thereby increasing ISF yield.[82–84] No data were collected regarding donor hydration status or skin temperature in the current study, as specific extraction yields or rates were not a key consideration for the nanoMIP measurements of cTnI.

Inflammatory responses induced by ISF extraction techniques, particularly those that disrupt the epidermal layer, can also influence biomarker concentrations. Extraction devices may disrupt capillary endothelial integrity, resulting in ''leaky'' junctions that reduce the size-selective transport of biomarkers across the capillary interface.[15,76,85] Moreover, ISF extraction can trigger localized inflammation, leading to elevated concentrations of inflammatory markers in the collected fluid. For example, Sjöbom *et al.* found that specific inflammatory markers were enriched in ISF obtained *via* blister suction extraction compared to plasma, reflecting a localized skin response to the extraction process.[26] In contrast, this study employed electroporation technology, which is non-invasive and specifically designed to avoid triggering local immune responses or elevating inflammatory biomarker levels.[86] This non-invasive ISF extraction is critical for maintaining sample integrity and assay reliability. Overall, there remains a need for standardized sampling protocols and careful interpretation of ISF biomarker data to ensure diagnostic accuracy, reproducibility, and clinical utility. Despite these sources of variability, we believe the robustness of the nanoMIPs used in our sensor platform enables reliable performance across a range of ISF conditions, particularly when paired with a non-invasive extraction device that does not trigger inflammation. The nanoMIP's high environmental stability and affinity for cTnI support the sensor's capacity to handle physiological variation while maintaining diagnostic accuracy.

Ultimately, this study demonstrates the high potential for a PoC diagnostic device for ACS that integrates a nanoMIP-based thermal sensor with wearable ISF extraction technology. The thermal sensing platform is capable of being miniaturized, and future work will focus on developing a standalone, fully portable device suitable for use in clinical settings. A prototype system will require comprehensive calibration to reliably translate R_{th} to cTnI concentration in patient samples, with results displayed *via* a simplified digital readout. The nanoMIP-functionalized SPEs are low-cost and disposable, enabling single-use operation for each measurement. Moreover, the high environmental stability of nanoMIPs allows for extended shelf life and eliminates the need for cold storage.[45]

4. Conclusion

In summary, we present a nanoMIP-based thermal sensor for the detection of cTnI in human ISF. The device accurately measured cTnI across the physiologically relevant range (0.1–1000 pg mL^{-1}) with simple operation, a 15–20 min measurement time, and a required sample volume of only 120 μL. The sensor also exhibited an excellent LoD in ISF (1.85 ± 0.32 pg mL^{-1}), showing favorable performance in this complex biological matrix. This LoD is significantly lower than that of gold-standard immunoassays currently utilized in healthcare (∼30 pg mL^{-1}), which demonstrates the high clinical relevance of the nanoMIP sensor. Similar thermal responses were observed when experiments were repeated using the same concentrations of cTnI-spiked serum and plasma, suggesting comparable levels of non-specific binding across all sample fluids. Additionally, the serum and plasma measurements also yielded excellent LoDs of 1.80 ± 0.22 and 1.78 ± 0.28 pg mL^{-1}, respectively, further highlighting the exceptional sensitivity and versatility of the nanoMIP-based thermal sensor.

Our study shows the feasibility of detecting cTnI in human ISF for the first time, offering a promising avenue for clinical application. The ability to distinguish between different concentrations of cTnI in ISF, coupled with the minimal variation compared to other sample fluids, underscores the potential for utilizing ISF measurements in various medical contexts. This methodology could be instrumental in developing a ''traffic light'' system for continuous or batch monitoring of cTnI levels, enabling rapid and informed decision-making by healthcare professionals without requiring invasive blood draws, sample processing, or laboratory-based immunoassays. Furthermore, the potential to create nanoMIP-based portable sensors combined with ISF extraction for PoC detection could revolutionize emergency response scenarios, providing first responders with quick and actionable information for chest pain assessment and subsequent treatment decisions. Ultimately, this could

improve patient outcomes, reduce healthcare burdens, and contribute to the drive toward personalized healthcare.

Author contributions

Joshua Saczek: investigation, methodology, validation, formal analysis, writing – original draft, visualization. Amy Dann: investigation, writing – review & editing, visualization. Robert D. Crapnell: resources, writing – review & editing. Craig E. Banks: resources, writing – review & editing. Rhiannon E. Johnson: investigation, resources, writing – review & editing. Francesco Canfarotta: investigation, resources, writing – review & editing. Alan Thomson: investigation, resources, writing – review & editing. Azfar Zaman: writing – review & editing, supervision. Ioakim Spyridopoulos: writing – review & editing, supervision, funding acquisition. Katarina Novakovic: writing – review & editing, supervision, project administration, funding acquisition. Marloes Peeters: conceptualization, methodology, writing – review & editing, supervision. Jake McClements: conceptualization, methodology, writing – review & editing, supervision, project administration, funding acquisition.

Conflicts of interest

The authors declare no conflict of interest.

Data availability

The data supporting this article have been included as part of the supplementary information (SI). Supplementary information is available. See DOI: https://doi.org/10.1039/d5nh00441a.

The data that support the findings of this study are available from the corresponding author upon reasonable request.

Acknowledgements

JM, IS, and KN would like to acknowledge funding from the Northern Accelerator Feasibility Award for consumables and salary for JS. AD's salary was supported through the USDA National Institute of Food and Agriculture, AFRI project NIFA 2022-67021-36408. The authors thank KIFFIK Biomedical Inc. for supplying ISF samples and technical support.

References

1 British Heart Foundation, *Global Heart & Circulatory Diseases Factsheet September 2024*, 2024.
2 N. Ojha and A. S. Dhamoon, *StatPearls*, StatPearls Publishing Copyright © 2024, StatPearls Publishing LLC., Treasure Island (FL), 2024.
3 G. De Luca, H. Suryapranata, J. P. Ottervanger and E. M. Antman, *Circulation*, 2004, **109**, 1223–1225.
4 R. Bingisser, C. Cairns, M. Christ, P. Hausfater, B. Lindahl, J. Mair, M. Panteghini, C. Price and P. Venge, *Am. J. Emerg. Med.*, 2012, **30**, 1639–1649.
5 L. Zhang, Z. H. Liu, Y. J. Lv, S. Fu, Z. M. Luo and M. L. Guo, *BMC Med. Inf. Decis. Making*, 2023, **23**, 292.
6 L.-N. Ghilencea, M.-R. Chiru, M. Stolcova, G. Spiridon, L.-M. Manea, A.-M. A. Stănescu, A. Bokhari, I. D. Kilic, G. G. Secco, N. Foin and C. Di Mario, *Front. Cardiovasc. Med.*, 2022, **9**, 868635.
7 E. Cross, S. How and S. Goodacre, *Emerg. Med. J.*, 2007, **24**, 100–102.
8 J. Stepinska, M. Lettino, I. Ahrens, H. Bueno, L. Garcia-Castrillo, A. Khoury, P. Lancellotti, C. Mueller, T. Muenzel, A. Oleksiak, R. Petrino, M. R. Guimenez, D. Zahger, C. J. M. Vrints, S. Halvorsen, E. de Maria, G. Y. H. Lip, R. Rossini, M. Claeys and K. Huber, *Eur. Heart J. Acute Cardiovasc. Care*, 2020, **9**, 76–89.
9 B. Yousaf, S. Alexander, W. Scott and K. Sadia, *BMJ Open Quality*, 2019, **8**, e000629.
10 K. C. Park, D. C. Gaze, P. O. Collinson and M. S. Marber, *Cardiovasc. Res.*, 2017, **113**, 1708–1718.
11 M. S. Rice and D. C. MacDonald, *J. Am. Board Fam. Pract.*, 1999, **12**, 214–218.
12 P. Bollella, S. Sharma, A. E. G. Cass and R. Antiochia, *Electroanalysis*, 2019, **31**, 374–382.
13 B. Venkatesh, T. J. Morgan and J. Cohen, *Crit. Care Med.*, 2010, **38**, S630–S636.
14 N. Fogh-Andersen, B. Altura, B. T. Altura and O. Siggaard-Andersen, *Clin. Chem.*, 1995, **41**, 1522–1525.
15 M. Friedel, I. A. P. Thompson, G. Kasting, R. Polsky, D. Cunningham, H. T. Soh and J. Heikenfeld, *Nat. Biomed. Eng.*, 2023, **7**, 1541–1555.
16 Z. Wu, Z. Qiao, S. Chen, S. Fan, Y. Liu, J. Qi and C. T. Lim, *Commun. Mater.*, 2024, **5**, 33.
17 J. Jathar, H. Mahajan and P. Nerkar, *Ann. Pharm. Fr.*, 2024, **82**, 953–965.
18 J. A. Stenken, M. K. Church, C. A. Gill and G. F. Clough, *AAPS J.*, 2010, **12**, 73–78.
19 E. Abado, T. Aue and H. Okon-Singer, *Front. Psychiatry*, 2021, **12**, 678891.
20 M. K. Tuck, D. W. Chan, D. Chia, A. K. Godwin, W. E. Grizzle, K. E. Krueger, W. Rom, M. Sanda, L. Sorbara, S. Stass, W. Wang and D. E. Brenner, *J. Proteome Res.*, 2009, **8**, 113–117.
21 C. Wei, D. Fu, T. Ma, M. Chen, F. Wang, G. Chen and Z. Wang, *Biosens. Bioelectron.*, 2024, **258**, 116326.
22 X. Zhang, G. Chen, F. Bian, L. Cai and Y. Zhao, *Adv. Mater.*, 2019, **31**, 1902825.
23 X. Yuan, O. Ouaskioud, X. Yin, C. Li, P. Ma, Y. Yang, P.-F. Yang, L. Xie and L. Ren, *Micromachines*, 2023, **14**, 1452.
24 S. M. Albelda, P. M. Sampson, F. R. Haselton, J. M. McNiff, S. N. Mueller, S. K. Williams, A. P. Fishman and E. M. Levine, *J. Appl. Physiol.*, 1988, **64**, 308–322.
25 J. A. Cooper, P. J. D. Vecchio, F. L. Minnear, K. E. Burhop, W. M. Selig, J. G. Garcia and A. B. Malik, *J. Appl. Physiol.*, 1987, **62**, 1076–1083.
26 U. Sjöbom, K. Christenson, A. Hellström and A. K. Nilsson, *Front. Immunol.*, 2020, **11**, 597632.
27 S. Sharma, P. Jackson and J. Makan, *Cardiac troponins*, BMJ Publishing Group, 2004.
28 D. C. Gaze and P. O. Collinson, *Ann. Clin. Biochem.*, 2008, **45**, 349–355.

29 H. Mirzajani, P. Zolfaghari, B. Y. Koca and H. Urey, *ACS Sens.*, 2025, DOI: 10.1021/acssensors.5c01691.
30 B. J. Vermeer, F. C. Reman and C. M. van Gent, *J. Invest. Dermatol.*, 1979, **73**, 303–305.
31 A. Oharazawa, G. Maimaituxun, K. Watanabe, T. Nishiyasu and N. Fujii, *J. Dermatol. Sci.*, 2024, **114**, 141–147.
32 B. Q. Tran, P. R. Miller, R. M. Taylor, G. Boyd, P. M. Mach, C. N. Rosenzweig, J. T. Baca, R. Polsky and T. Glaros, *J. Proteome Res.*, 2018, **17**, 479–485.
33 T. U. Consortium, *Nucleic Acids Res.*, 2022, **51**, D523–D531.
34 T. Young, V. Clark, N. Arroyo-Currás and J. Heikenfeld, *ECS Sens. Plus*, 2023, **2**, 027001.
35 G. Luc, Z. Majd, P. Poulain, L. Elkhalil and J. C. Fruchart, *Atherosclerosis*, 1996, **127**, 131–137.
36 G. Florea, I. F. Tudorache, E. V. Fuior, R. Ionita, M. Dumitrescu, I. M. Fenyo, V. G. Bivol and A. V. Gafencu, *Biomedicines*, 2022, 10.
37 K. M. Saifullah and Z. Faraji Rad, *Adv. Mater. Interfaces*, 2023, **10**, 2201763.
38 J. Korf, K. D. Huinink and G. A. Posthuma-Trumpie, *Trends Biotechnol.*, 2010, **28**, 150–158.
39 R. D. Crapnell, F. Canfarotta, J. Czulak, R. Johnson, K. Betlem, F. Mecozzi, M. P. Down, K. Eersels, B. van Grinsven, T. J. Cleij, R. Law, C. E. Banks and M. Peeters, *ACS Sens.*, 2019, **4**, 2838–2845.
40 K. Haupt and K. Mosbach, *Trends Biotechnol.*, 1998, **16**, 468–475.
41 S. Garg, P. Singla, S. Kaur, R. D. Crapnell, C. E. Banks, S. Seyedin and M. Peeters, *Small*, 2024, 2403320.
42 S. Choudhary and Z. Altintas, *Biosensors*, 2023, **13**, 229.
43 F. Canfarotta, A. Poma, A. Guerreiro and S. Piletsky, *Nat. Protoc.*, 2016, **11**, 443–455.
44 J. McClements, P. M. Seumo Tchekwagep, A. L. Vilela Strapazon, F. Canfarotta, A. Thomson, J. Czulak, R. E. Johnson, K. Novakovic, P. Losada-Pérez, A. Zaman, I. Spyridopoulos, R. D. Crapnell, C. E. Banks and M. Peeters, *ACS Appl. Mater. Interfaces*, 2021, **13**, 27868–27879.
45 J. McClements, L. Bar, P. Singla, F. Canfarotta, A. Thomson, J. Czulak, R. E. Johnson, R. D. Crapnell, C. E. Banks, B. Payne, S. Seyedin, P. Losada-Pérez and M. Peeters, *ACS Sens.*, 2022, **7**, 1122–1131.
46 J. Saczek, O. Jamieson, J. McClements, A. Dann, R. E. Johnson, A. D. Stokes, R. D. Crapnell, C. E. Banks, F. Canfarotta, I. Spyridopoulos, A. Thomson, A. Zaman, K. Novakovic and M. Peeters, *Biosens. Bioelectron.*, 2025, **282**, 117467.
47 *US Pat.*, 2018.
48 B. van Grinsven, K. Eersels, M. Peeters, P. Losada-Pérez, T. Vandenryt, T. J. Cleij and P. Wagner, *ACS Appl. Mater. Interfaces*, 2014, **6**, 13309–13318.
49 F. Canfarotta, J. Czulak, K. Betlem, A. Sachdeva, K. Eersels, B. van Grinsven, T. J. Cleij and M. Peeters, *Nanoscale*, 2018, **10**, 2081–2089.
50 Y. Yang and H. Zhao, *Appl. Surf. Sci.*, 2022, **577**, 151895.
51 L. K. Newby, R. L. Jesse, J. D. Babb, R. H. Christenson, T. M. De Fer, G. A. Diamond, F. M. Fesmire, S. A. Geraci, B. J. Gersh, G. C. Larsen, S. Kaul, C. R. McKay, G. J. Philippides and W. S. Weintraub, *J. Am. Coll. Cardiol.*, 2012, **60**, 2427–2463.
52 N. I. f. H. C. Excellence, High-sensitivity troponin tests for the early rule out of NSTEMI, https://www.nice.org.uk/guidance/DG40, (accessed 05/03/2024, 2024).
53 C. Galli and G. Lippi, *Ann. Transl. Med.*, 2016, **4**, 257.
54 M. Tada, H. Azuma, N. Yamada, K. I. Kano, H. Nagai, S. Maeda, H. Ishida, T. Aoyama, R. Okada, T. Kawano, T. Kobuchi, H. Uzui, H. Matano, H. Iwasaki, K. Maeno, Y. Shimada, H. Yoshida, M. Ando, Y. Murakami, N. Iwakami, S. Kishimoto, T. Iwami, H. Tada, A. Chapman, N. Mills, H. Hayashi, T. A. Furukawa and N. Watanabe, *BMJ Open*, 2019, **9**, e026985.
55 A. H. B. Wu, P. A. Kavsak, K. M. Aakre, R. H. Christenson, D. N. Greene, F. S. Apple, W. F. Peacock, J. E. Hollander, J. A. de Lemos, D. Morrow, J. Januzzi and A. S. Jaffe, *Clin. Chem.*, 2020, **66**, 1146–1149.
56 J. C. Brandmeier, K. Raiko, Z. Farka, R. Peltomaa, M. J. Mickert, A. Hlaváček, P. Skládal, T. Soukka and H. H. Gorris, *Adv. Healthcare Mater.*, 2021, **10**, e2100506.
57 B. D. Mansuriya and Z. Altintas, *Nanomaterials*, 2021, **11**, 578.
58 T.-H. Lee, L.-C. Chen, E. Wang, C.-C. Wang, Y.-R. Lin and W.-L. Chen, *Biosensors*, 2021, **11**, 210.
59 F. S. Apple, P. O. Collinson, P. A. Kavsak, R. Body, J. Ordonez-Llanos, A. K. Saenger, T. Omland, O. Hammarsten, A. S. Jaffe and IFCC Committee on Clinical Applications of Cardiac Bio-Markers, *Clin. Chem.*, 2021, **67**, 730–735.
60 I. V. L. Thulin, G. M. S. Myrmel, S. M. F. Jordalen, P. Collinson and K. M. Aakre, *J. Lab. Precis. Med.*, 2023, **8**, 20.
61 J. N. Chen, G. K. Hasabnis, E. Akin, G. Gao, S. P. Usha, R. Süssmuth and Z. Altintas, *Sens. Actuators, B*, 2024, **417**, 136052.
62 H. Fu, Z. Qin, X. Li, Y. Pan, H. Xu, P. Pan, P. Song and X. Liu, *ACS Sens.*, 2023, **8**, 3574–3584.
63 G.-R. Han, A. Goncharov, M. Eryilmaz, H.-A. Joung, R. Ghosh, G. Yim, N. Chang, M. Kim, K. Ngo, M. Veszpremi, K. Liao, O. B. Garner, D. Di Carlo and A. Ozcan, *ACS Nano*, 2024, **18**, 27933–27948.
64 A. Campu, I. Muresan, M. Potara, D. R. Lazar, F.-L. Lazar, S. Cainap, D. M. Olinic, D. Maniu, S. Astilean and M. Focsan, *J. Mater. Chem. B*, 2024, **12**, 962–972.
65 L. Koechlin, J. Boeddinghaus, P. Lopez-Ayala, C. Reber, T. Nestelberger, K. Wildi, C. C. Spagnuolo, I. Strebel, J. Glaeser, P. Bima, L. Crisanti, L. Herraiz-Recuenco, E. Dubach, Ò. Miró, F. J. Martin-Sanchez, D. Kawecki, D. I. Keller, M. Christ, A. Buser, M. R. Giménez, G. L. Størvold, M. N. Broughton, T. Omland, M. N. Lyngbakken, H. Røsjø, C. Mueller, D. Wussler, C. Puelacher, G. Huré, K. Rentsch, D. M. Gualandro, J. Reinhardt, A. Y. Sanchez, B. Okamura, S. Shrestha, P. Haaf, P. Badertscher, J. E. Walter, B. López, G. Martinez-Nadal, E. R. Adrada, J. Parenica, A. V. Eckardstein, B. Morawiec, P. Muzyk and H. Schirmer, *J. Am. Coll. Cardiol.*, 2024, **84**, 726–740.
66 B. McDonnell, S. Hearty, P. Leonard and R. O'Kennedy, *Clin. Biochem.*, 2009, **42**, 549–561.

67 S. Zahran, V. P. Figueiredo, M. M. Graham, R. Schulz and P. M. Hwang, *J. Appl. Lab. Med.*, 2018, **3**, 450–455.
68 J. Mathew, P. Sankar and M. Varacallo, *Physiology, Blood Plasma*, StatPearls, 2023.
69 O. Decaux, E. Laurat, A. Perlat, C. Cazalets, P. Jego and B. Grosbois, *Eur. J. Intern. Med.*, 2009, **20**, 457–461.
70 R. S. Rosenson, A. McCormick and E. F. Uretz, *Clin. Chem.*, 1996, **42**, 1189–1195.
71 M. Leeman, J. Choi, S. Hansson, M. U. Storm and L. Nilsson, *Anal. Bioanal. Chem.*, 2018, **410**, 4867–4873.
72 P. R. Miller, R. M. Taylor, B. Q. Tran, G. Boyd, T. Glaros, V. H. Chavez, R. Krishnakumar, A. Sinha, K. Poorey, K. P. Williams, S. S. Branda, J. T. Baca and R. Polsky, *Commun. Biol.*, 2018, **1**, 173.
73 N. N. Ahmad, N. N. N. Ghazali, A. T. Abdul Rani, M. H. Othman, C. C. Kee, P. K. Jiwanti, A. Rodríguez-Gómez and Y. H. Wong, *Micromachines*, 2023, **14**, 881.
74 L. M. Ebah, *Extraction and analysis of interstitial fluid, and characterisation of the interstitial compartment in kidney disease*, The University of Manchester (United Kingdom), 2012.
75 R. K. Reed and K. Rubin, *Cardiovasc. Res.*, 2010, **87**, 211–217.
76 P. P. Samant, M. M. Niedzwiecki, N. Raviele, V. Tran, J. Mena-Lapaix, D. I. Walker, E. I. Felner, D. P. Jones, G. W. Miller and M. R. Prausnitz, *Sci. Transl. Med.*, 2020, **12**, eaaw0285.
77 X. Ding and P. A. Heiden, *Macromol. Mater. Eng.*, 2014, **299**, 268–282.
78 J. Wackerlig and R. Schirhagl, *Anal. Chem.*, 2016, **88**, 250–261.
79 A. Basu, S. Dube, M. Slama, I. Errazuriz, J. C. Amezcua, Y. C. Kudva, T. Peyser, R. E. Carter, C. Cobelli and R. Basu, *Diabetes*, 2013, **62**, 4083–4087.
80 A. Himawan, L. K. Vora, A. D. Permana, S. Sudir, A. R. Nurdin, R. Nislawati, R. Hasyim, C. J. Scott and R. F. Donnelly, *Adv. Healthcare Mater.*, 2023, **12**, 2202066.
81 S. Kawakatsu, X. Liu, B. Tran, B. P. Tran, L. Manzanero, E. Shih, A. Shek and J. J. Lim, *J. Diabetes Sci. Technol.*, 2022, **16**, 1183–1189.
82 M. Pawlaczyk, M. Lelonkiewicz and M. Wieczorowski, *Post-epy Dermatol. Alergol.*, 2013, **30**, 302–306.
83 G. B. Jemec and J. Serup, *Acta Derm.-Venereol.*, 1990, **70**, 245–247.
84 Z. Pu, X. Zhang, H. Yu, J. Tu, H. Chen, Y. Liu, X. Su, R. Wang, L. Zhang and D. Li, *Sci. Adv.*, 2021, **7**, eabd0199.
85 F. Ribet, A. Bendes, C. Fredolini, M. Dobielewski, M. Böttcher, O. Beck, J. M. Schwenk, G. Stemme and N. Roxhed, *Adv. Healthcare Mater.*, 2023, **12**, 2202564.
86 K. B. Inc., *CONTINUOUS ACCESS TO INTERSTITIAL FLUID Potential uses in diagnostics and drug development*, 2022.

